



Elongated titania nanostructures as efficient photocatalysts for degradation of selected herbicides

Mila Vranješ^a, Zoran V. Šaponjić^a, Ljiljana S. Živković^a, Vesna N. Despotović^b, Daniela V. Šojić^b, Biljana F. Abramović^{b,**}, Mirjana I. Čomor^{a,*}

^a Vinča Institute of Nuclear Sciences, University of Belgrade, P.O. Box 522, 11001 Belgrade, Serbia

^b Department of Chemistry, Biochemistry and Environmental Protection, Faculty of Sciences, University of Novi Sad, Trg D. Obradovića 3, 21000 Novi Sad, Serbia

ARTICLE INFO

Article history:

Received 28 March 2014

Received in revised form 3 June 2014

Accepted 6 June 2014

Available online 13 June 2014

Keywords:

Titania nanotubes

Hydrothermal synthesis

Annealing

Herbicides

Photocatalysis

ABSTRACT

Titanium dioxide nanotubes (TNT) were synthesized via hydrothermal method and calcined at various temperatures. The obtained calcined TiO₂ nanomaterials with specific elongation orientation were characterized by transmission and scanning electron microscopy (TEM, SEM), X-ray diffraction (XRD), UV/Vis diffuse reflection spectroscopy (DRS), Laser Doppler electrophoresis (LDE) and their textural properties were evaluated. The photocatalytic activity of obtained nanopowders was evaluated considering photodegradation rate of herbicide clomazone, rarely studied herbicide. The influence of calcination temperature of catalysts with elongated morphology on their photocatalytic activity was evaluated. The best results were obtained with TNT annealed at 700 °C, which can be assigned to the best balance between crystal structure, morphology and surface properties of nanoparticles induced by annealing. Also, the photocatalytic degradation rates of another two herbicides (picloram, and mecoprop) were compared, due to possibility that the efficiency of photocatalytic degradation is greatly influenced by the molecular structure. The mineralization degree of selected herbicides in the presence of TiO₂ based photocatalysts was evaluated applying total organic carbon (TOC) measurements.

© 2014 Elsevier B.V. All rights reserved.

1. Introduction

Nanocrystalline TiO₂ has attracted great interest in last few decades due to their unique properties, crystal structures, morphologies and promising applications in various fields, such as dye sensitized solar cells, photocatalysis, sensing and optoelectronic devices [1]. The TiO₂ is mainly used as photocatalytic material in the processes of water and air purification due to excellent photo and chemical stability, nontoxicity, superior redox ability and low cost [2]. The performances of TiO₂ nanomaterial are highly dependent on its crystal structure, size and shape [3,4]. The ability to control the size and shape of TiO₂ nanoparticles is becoming an important scope in materials science because it opens up the possibility to combine high aspect ratio, high surface area and versatile chemistry for efficient photoinduced charge separation [5]. Since discovery of carbon nanotubes, much effort has been directed towards synthesis

of one-dimensional (1D) nanostructures like rods, wires, tubes and belts due to their shape and size dependent optical and electrical properties [6]. Convenient hydrothermal synthetic route applied for synthesis of titania nanotubes (TNT), using highly basic dispersion of TiO₂ nanoparticles as a precursor, was the most commonly applied method in the last decade [7,8]. These nanotubes were further used as a precursor for synthesis of anisotropic (1D) TiO₂ nanocrystals of different crystal structures capable of vectorial electron transport necessary for creating efficient photoconversion systems [9].

Recently, 1D titania nanocrystals have been used as photocatalysts for degradation of different persistent organic pollutants as reviewed by Liu and coauthors [10]; usually dyes were used as test molecules for obtaining degradation capabilities of photocatalysts, herbicides not yet in a greater extent. Hazardous contaminants such as pesticides constitute a serious risk for human health due to their high toxicity. The widespread use of pesticides can result in contamination of surface and ground waters in the areas of their application [11]. Furthermore, bioaccumulation and biomagnification can lead to hazardous concentrations in humans. Among the chemicals that are likely to be found in groundwater, pesticides have a non-negligible presence and their elimination is

* Corresponding author. Tel.: +381 11 380 41 92; fax: +381 11 3408 607.

** Corresponding author. Tel.: +381 21 485 27 53; fax: +381 21 454 065.

E-mail addresses: biljana.abramovic@dh.uns.ac.rs (B.F. Abramović), mirjanac@vinca.rs (M.I. Čomor).

necessary, especially if the water is intended for human consumption. Advanced oxidation processes have provided a promising alternative for the remediation of contaminated water when compared to other treatment methods [12,13], while heterogeneous photocatalysis by TiO_2 appeared as one of the most efficient methods for the elimination of a number of pesticides from water [14,15].

This paper is mainly devoted to characterization of elongated titania nanoparticles obtained by calcination of hydrothermally synthesized TNTs, in the range of temperatures from 400 to 800 °C. The obtained calcined TNTs with specific elongation orientation are characterized by transmission and scanning electron microscopy (TEM, SEM), X-ray diffraction (XRD), UV/Vis diffuse reflection spectroscopy (DRS), Laser Doppler electrophoresis (LDE) and their texture properties were attained. We have further studied the influence of heat transformation of TNTs on their photocatalytic activity following decomposition rates and mineralization of herbicide clomazone (2-[(2-chlorophenyl)methyl]-4,4-dimethyl-3-isoxazolidinone, Table 1) highly water soluble herbicide which can cause ground water contamination [16]. Also, in order to obtain the link between photocatalysts activity and molecular structure of the substrates, the photocatalytic activity of picloram (4-amino-3,5,6-trichloro-2-pyridin carboxylic acid) and mecoprop (RS-2-(4-chloro-o-tolyloxy)propionic acid) (Table 1) were studied. They were chosen because of their wide use in selective control of many annual and some perennial weeds, and because of their occurrence in drinking water [17,18].

2. Experimental

Chemicals: TiO_2 powder (p.a., Fluka), clomazone (2-[(2-chlorophenyl)methyl]-4,4-dimethyl-3-isoxazolidinone Table 1) (98.8%, Riedel-de Haën) and picloram (4-amino-3,5,6-trichloro-2-pyridincarboxylic acid, Table 1) (99.4%, pestanal quality, Riedel-de Haën), H_3PO_4 (85% Lachema), acetonitrile (ACN) (99.8%, J.T. Baker), H_2SO_4 (conc., Aldrich), NaOH (ZorkaPharm), HCl (conc. Aldrich) were used without further purification. The commercial herbicide mecoprop (RS-2-(4-chloro-o-tolyloxy)propionic acid, Table 1), 98% purity, obtained from the Chemical Factory “Župa” Kruševac, Serbia, was purified by conventional recrystallization from water–ethanol (1:1, v/v) solution. Milli-Q deionized water was used as a solvent. Air and argon gases were of high purity (99.5%). As reference material the TiO_2 Degussa P25 (75% anatase and 25% rutile form, 50 m^2/g , about 20 nm, non-porous, hereafter P25) was used. The pH of water suspension of P25, as prepared and annealed TNT-700 was ~5.6, 9 and 7.8, respectively.

Computer modeling procedures used in this study were performed using Hyperchem 8.0.6 (Hypercube Inc.). The compounds formulae were entered into the data set as two-dimensional sketches into Hyperchem. Full optimization geometry and calculation of the positive and negative molecular electrostatic potentials MEPs for the best conformer were performed using the semi-empirical method AM1 running on Hyperchem. Electronic properties were computed from single point calculations.

2.1. Synthesis of TiO_2 nanotubes

Titania nanotubes were synthesized by a hydrothermal treatment (48 h/120 °C) of TiO_2 powder (Fluka) used as a precursor in proton deficient aqueous solution (10 mol/dm^3 NaOH) without shaking [7,8,19]. After autoclaving in Teflon vessel, the ensuing powder was separated from the solution using centrifuge. The powder was washed once using 1 mol/dm^3 HCl aqueous solution for 2 h and then several times using pure water. This washing procedure with water was repeated until the water reached pH = 7. Finally, the powder was separated from the washing solution by centrifugation.

Synthesized nanotubes were dried at 70 °C until attainment of constant weight. Portions of TNT powder were calcined in an oven, at 400, 500, 600, 700, and 800 °C.

2.2. Characterization of TNTs

XRD patterns of the TNT were obtained using standard powder diffraction methods with a Philips PW1830 X-ray powder diffractometer using $\text{Cu K}\alpha$ line. Phase composition (anatase/rutile) was estimated using characteristic diffraction peaks: for anatase (101) and for rutile (110).

The sizes and shapes of the used titania nanoparticles were determined using TEM, Hitachi H-7000 FA TEM operated at 125 kV. TEM samples were prepared by ultrasound treatment of particles water dispersion for 10 min in an ultrasound bath before drop-wise placing volume of 6 μl onto a holey carbon film supported on a copper grid. The specimen was air-dried overnight. A scanning electron microscope JEOL JSM 6460 LV and field emission scanning electron microscopy (FESEM) TESCAN Mira3 XMU at 20 kV were used to characterize the morphology of the titania powders. Gold-coated particles were examined on a SEM, JSM-6460LV JOEL instrument, operated at an accelerating voltage of 25 keV.

UV/Vis spectroscopy was performed using Thermo Scientific Evolution 600 UV–Vis spectrophotometer.

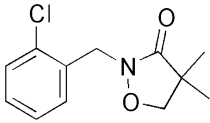
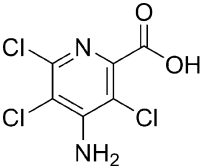
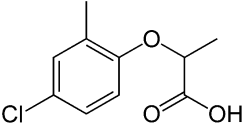
Nitrogen adsorption–desorption isotherms, for obtaining texture properties of the samples, were collected on a Micromeritics ASAP 2020 surface area and pore size analyzer at 77 K. Prior to adsorption, the samples were degassed at 423 K for 10 h, under a reduced pressure. The specific surface area of the samples was calculated by applying the Brunauer–Emmet–Teller (BET) equation from the linear part of the adsorption isotherm. The total pore volumes of micro and meso pores were obtained from the N_2 adsorption at $p/p_0 = 0.998$.

Zeta potential (ζ) of TNT nanoparticles was measured by Zeta-Sizer Nano ZS with 633 nm He-Ne laser (Malvern, UK), utilizing electrophoretic light scattering method [20]. The ζ -potential was calculated by instrument software, applying the Henry equation and the Smoluchowski approximation, from the electrophoretic mobility of particles measured by laser Doppler velocimetry. Series of dispersion samples containing 1 mg TNT/1 cm^3 NaCl (1×10^{-3} mol/dm^3) as inert electrolyte [21], were shaken for 24 h at room temperature. The as-prepared and calcined TNT were used. The ζ -potential measurements were performed in duplicate in the pH range from ~9 to ~3, and the average data presented.

2.3. Photodegradation procedure

The photocatalytic degradation of substrates were carried out in a cell made of Pyrex glass (total volume of ca. 40 cm^3 , liquid layer thickness 35 mm), with a plain window on which the light beam was focused. The cell was equipped with a magnetic stirring bar and a water circulating jacket. A 125 W high-pressure mercury lamp (Philips, HPL-N, emission bands in the UV region at 304, 314, 335, and 366 nm, with maximum emission at 366 nm), together with an appropriate concave mirror, was used as the radiation source. In a typical experiment, and unless otherwise stated, the initial herbicides concentration was 5.0×10^{-2} mmol/dm^3 , and the TiO_2 loading was 1.0 mg/cm^3 . The total suspension volume was 20 cm^3 . The aqueous suspension of TiO_2 was sonicated (50 Hz) in the dark for 15 min before illumination, to uniformly disperse the photocatalyst particles and attain adsorption equilibrium. The suspension thus obtained was thermostated at 25 ± 0.5 °C and then irradiated at a constant stream of O_2 (3.0 cm^3/min). During the irradiation, the mixture was stirred at a constant speed. The initial pH of reaction mixture clomazone, picloram and mecoprop in the presence of TNT were ~7.8, 7.2, and 7.4, respectively, while in the presence of

Table 1
Structural formulas of the herbicides.

Clomazone	Picloram	Mecoprop
		

P25 were ~5.5, 4.7, and 5.3. The photocatalytic degradations were performed at a natural pH in the case with TNT, and at pH 8 in the case with P25 (pH of the reaction mixture was adjusted by adding a dilute aqueous solution NaOH). The control experiments carried out under O₂ flow but by stopping the irradiation, showed that there were no losses of volatile compounds during the degradation.

2.4. Analytical procedure

For the LC–DAD kinetic studies of the herbicides photodegradation, samples of 0.50 cm³ of the reaction mixture were taken at the beginning of the experiment and at regular time intervals. Aliquot sampling caused a maximum volume variation of ca. 10% in the reaction mixture. The obtained suspensions were filtered through a Millipore (Millex-GV, 0.22 μm) membrane filter. The absence of the herbicide adsorption on the filters was preliminarily checked. After that, a 20 μL sample was injected and analyzed on an Agilent Technologies 1100 Series liquid chromatograph, equipped with a UV–vis DAD set at absorption maximum (210 nm for clomazone, 224 nm for picloram and 228 nm for mecoprop) and a Zorbax Eclipse XDB-C18 (150 mm × 4.6 mm i.d., particle size 5 μm, 25 °C) column. The mobile phase (flow rate 1 cm³/min) was a mixture of ACN and water (6:4, v/v, pH 3.97 for clomazone, 3:7, v/v, pH 2.56 for picloram, 1:1, v/v, pH 2.68 for mecoprop), the water being acidified with 0.1% H₃PO₄. In repeated runs, the results agreed within 3–10%.

The total organic carbon (TOC) analysis was performed on an Elemental Liqui TOC II according to Standard US EPA Method 9060A.

3. Results and discussion

For obtaining high quality TiO₂ elongated nanocrystals we used titania nanotubes as a precursor. Fig. 1a presents TEM image of titania nanotubes hydrothermally synthesized according to modified procedure of Kasuga et al. [7,8]. Reasonably uniform size distribution of nanotubes with outer diameter of about 10 nm and length that varies was observed. Peaks appearing in XRD patterns of as prepared nanotubes at 2θ = 25.4, 38, 48.3, 54, 55.2 and 62.9 deg., Fig. 1b, can be undoubtedly indexed as the anatase TiO₂ crystal planes: 101, 004, 200, 105, 211 and 204, respectively (JCPDS No. 21-1272). The appearance of reflection at 2θ = 24.5 deg. suggests existence of monoclinic TiO₂ (B) structure (PDF 74-1940) usually described as built-up from corner- and edge-sharing octahedra, similarly to the anatase titanium dioxide [20,22]. On the other hand, this peak could be also assigned to hydrogen titanate [23]. Both compounds follow anatase structure of nanotubes synthesized using hydrothermal method.

Titania nanotubes are ideal starting material for reshaping, i.e., obtaining high quality titanium dioxide nanocrystals of different shapes, sizes and crystalline structures applying calcination at different temperatures. Depending on their size and shape, these nanostructures exhibit different domains of crystallinity, surface areas and aspect ratios. Also, it should be stressed that washing procedure has a great importance on the Na content, titanates

formation, thermal stability and consequently on morphology of TNTs [24,25].

In Fig. 2, XRD patterns of titania nanotubes calcined at different temperatures (TNT-400–800) are presented. The development of the clear anatase crystalline phase with characteristic peaks in XRD patterns at 2θ = 25.5, 37, 38, 39, 48, 54, 55, 62, 63, 69, 70, 74–76 deg. (JCPDS No. 21-1272) was observed confirming that our washing procedure was properly chosen.

In the XRD pattern of the sample TNT-600, the appearance of the low intensity reflection at 2θ = 28 deg. suggested the initiation of the rutile phase formation. Calcination temperature increased to 700 °C induced further development of rutile crystalline phase (5%) which was confirmed by the increased intensity of the peak at 2θ = 28 deg. in the XRD pattern of the sample TNT-700. In the

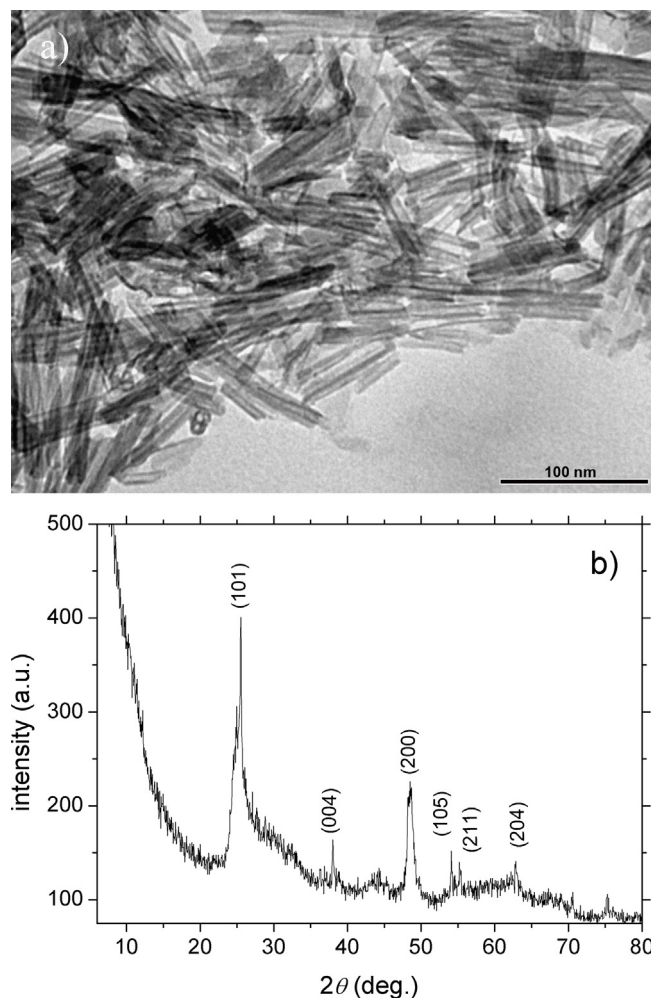


Fig. 1. TEM image (a) and XRD pattern with Miller indexes assigned to corresponding peaks (b) of as prepared TNT.

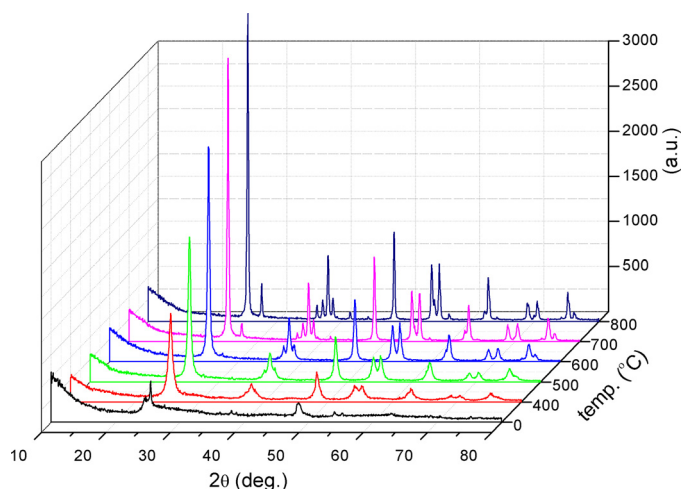


Fig. 2. XRD patterns of calcined TNTs; calcination temperature presented as a z-axis.

sample TNT-800, calcined at 800 °C, the crystal phase composition consists of anatase and approximately 10% of rutile.

The changes in morphology of titania nanotubes calcined in a temperature range from 400 to 800 °C were analyzed by FESEM and SEM, Fig. 3. FESEM/SEM images of TNT-400, TNT-600, TNT-700 and TNT-800 samples show that their morphology is significantly affected by the calcinations temperature. Similar observations of the changes of phase structure and crystallite size of the nanotubes before and after calcinations at different temperatures (300–900 °C) were reported in the literature [26].

The FESEM image of nanotubes calcined at 400 °C, Fig. 3a, reveals pretty much uniform cylindrical morphology of nanocrystals whose diameter is around 13 nm while the length varies

Table 2
Textural analysis.

Sample	S_p (m ² /g)	V_{total} (cm ³ /g)	D_m (nm)
TNT	182.33	0.3963	6.8
TNT-600	37.34	0.2745	31.7
TNT-700	15.81	0.0492	14.8
TNT-800	11.99	0.0267	9.1

S_p —specific surface area.

V_{total} —the total pore volume.

D_m —mean pore diameter.

until few hundred nanometers. In the morphology of the sample calcined at 600 °C, Fig. 3b, cylindrical shape predominate but the average outer diameter is slightly higher, 15 nm, while the length is little bit shorter in comparison to nanocrystals calcined at 400 °C. In the sample calcined at 700 °C, reasonably uniform nanorods observed which have diameter of 59 nm and length between 400 and 500 nm. The morphology of the sample calcined at 800 °C, completely changed in comparison to previously mentioned. Nanoparticles with almost bimodal size distribution of 71 and 91 nm were obtained (Fig. 3d). Cylindrical morphology in this sample completely disappeared and also the particles agglomeration increased, according to SEM image (Fig. 3d). Despite significant changes in morphology between as prepared and calcined TNT, almost no changes in UV/Vis reflection spectra can be observed. All samples had absorption threshold at about 3.2 eV (Fig. 4). Only TNT-700 and TNT-800 have sharp decrease of reflection moved to longer wavelengths induced by rutile crystalline phase present in the samples.

The data obtained from textural analysis of titania nanotubes before calcination and titania nanotubes calcined at 600, 700 and 800 °C are given in Table 2. The observed decrease in the specific surface area and total pore volumes of TNT samples by increasing

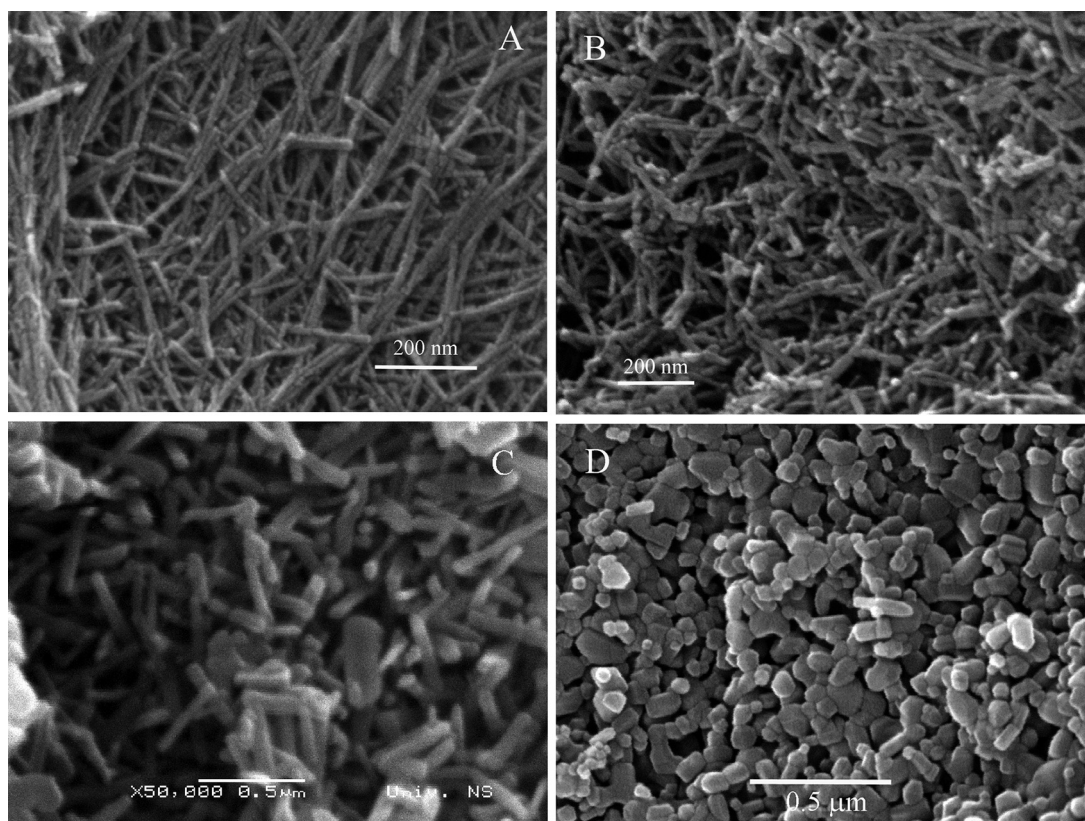


Fig. 3. A typical FESEM and SEM images of calcined TNT samples at different temperatures: (a) 400 °C (FESEM), (b) 600 °C (FESEM), (c) 700 °C (SEM) and (d) 800 °C (FESEM).

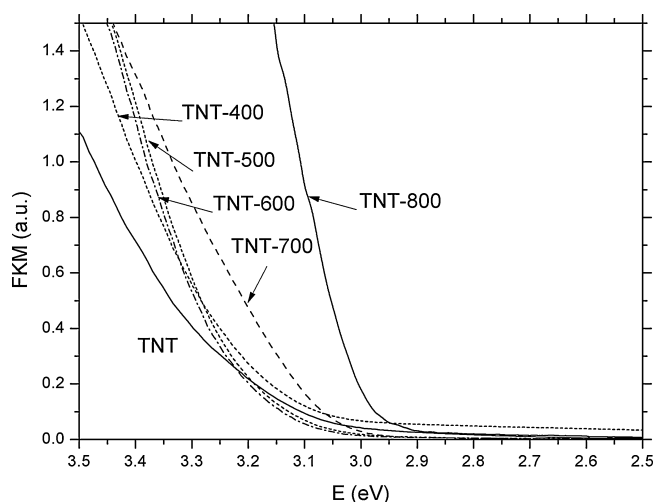


Fig. 4. UV/Vis DRS of as prepared and annealed TNT photocatalysts.

calcinations temperatures is expected and is in agreement with FESEM measurements. The N_2 -sorption isotherms (not shown) of all samples exhibited hysteresis loop at high p/p_0 values. Multiple reductions of specific surface areas and total pore volumes after calcinations at 700 and 800 °C confirmed the partial sintering of the samples or annealing-induced structural collapse.

In our previous work we studied photocatalytic degradation process of clomazone in the presence of commercial TiO_2 powders [16]. In this work we had intention to analyze influence of structure and shape of TiO_2 on photocatalytic activity in the degradation process of clomazone as rarely studied herbicide. The photocatalytic efficiency of as synthesized titania nanotubes and nanotubes calcined in the temperature range from the 400 to 800 °C, in the process of degradation of clomazone dispersed in water under UV irradiation was investigated, Fig. 5. All calcined samples showed higher photocatalytic efficiency compared to as prepared TNT. Photocatalytic efficiency of calcined samples increased with the increase of the degree of crystallinity. This finding is in accordance with our previous work [27]. We concluded that increase of the crystallinity of TiO_2 nanoparticles followed by decrease in the number of surface Ti defect sites induced overall increase of their photocatalytic activity. Similar observations were made by

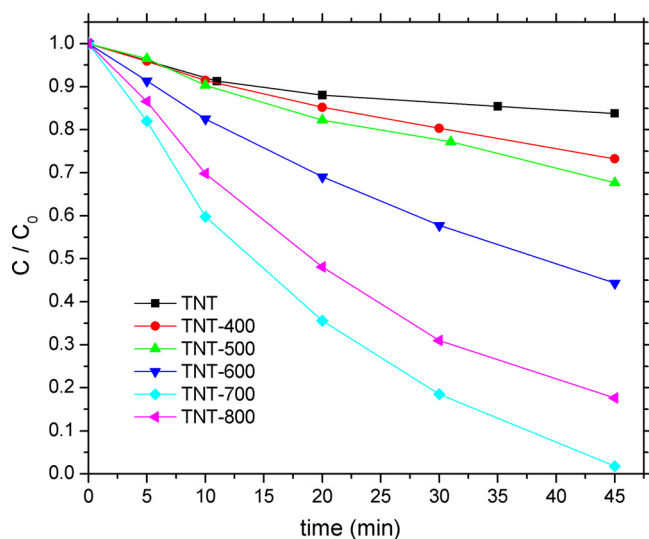


Fig. 5. The effect of calcination temperature on the efficiency of TNT (400–800) in the photocatalytic degradation of clomazone.

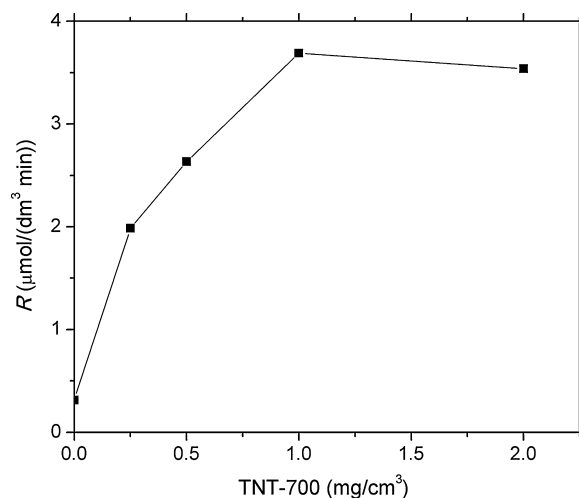


Fig. 6. The effect of TNT-700 loading on the degradation rate (R) determined after 20 min of irradiation.

Cropek et al. [28]. According to the obtained results it is obvious that the aqueous dispersion of titania nanotubes calcined at 700 °C and 800 °C showed the highest efficiency in the degradation of clomazone. These findings can be explained by appearance of rutile structure in already well-established anatase crystalline structure as can be seen in XRD patterns of these samples, Fig. 2. It is known that photocatalytic efficiency of TiO_2 is substantially increased in the sample containing both crystal phases (anatase and rutile) compared to single crystal sample [29]. Further increase of calcination temperature to 800 °C induced decrease of photocatalytic efficiency which is still higher compared to the as prepared titania nanotubes and samples calcined at temperatures lower than 700 °C. Such decrease in photocatalytic efficiency could be explained by the higher degree of particle agglomeration.

The effect of loading (from 0.25 to 2.00 mg/cm^3) of the most efficient photocatalyst, TNT 700, on the degradation rate of clomazone was examined, Fig. 6. Under the relevant experimental conditions, the reaction followed pseudo-first order kinetics. On the basis of the kinetic curves $\ln c$ (substrate concentration) vs. t , the values of the pseudo-first order rate constant k' were calculated. The degradation rate of clomazone (R) was calculated for all the investigated catalyst loadings as the product of k' and c_0 , where c_0 is the initial concentration of clomazone. As can be seen, the increase in the load of TNT up to 1.0 mg/cm^3 was accompanied by a rapid increase in the degradation rate, probably as a consequence of the overall increase of the number of active sites, which in turn increases the number of hydroxyl and superoxide radicals. However, the increase of the catalyst loading above the level of 1 mg/cm^3 had no significant effect on the photodegradation rate, which can be ascribed to the fact that almost all the light available, is already utilized.

The appearance of the plateau, and absence of a significant decrease in the removal efficiency, indicates that the light dissipation at higher catalyst's loading is not pronounced, which is a beneficial characteristic of this catalyst [30].

In order to examine the influence of the morphology and crystal structure of TiO_2 catalysts on their photocatalytic activity, the degradation processes of herbicides: clomazone, picloram and mecoprop were compared (Fig. 7). The photocatalytic activities of aqueous dispersions of several TiO_2 powders were compared: as prepared titania nanotubes, TNT-700 and P25. Since the pH has a great effect on the photodegradation efficiency of herbicides and it is one of the most influencing factors in heterogenous photocatalytic reactions [15], the pH values of dispersions were adjusted on pH ~8 for P25, pH ~7.2–7.8 for TNT-700, and finally

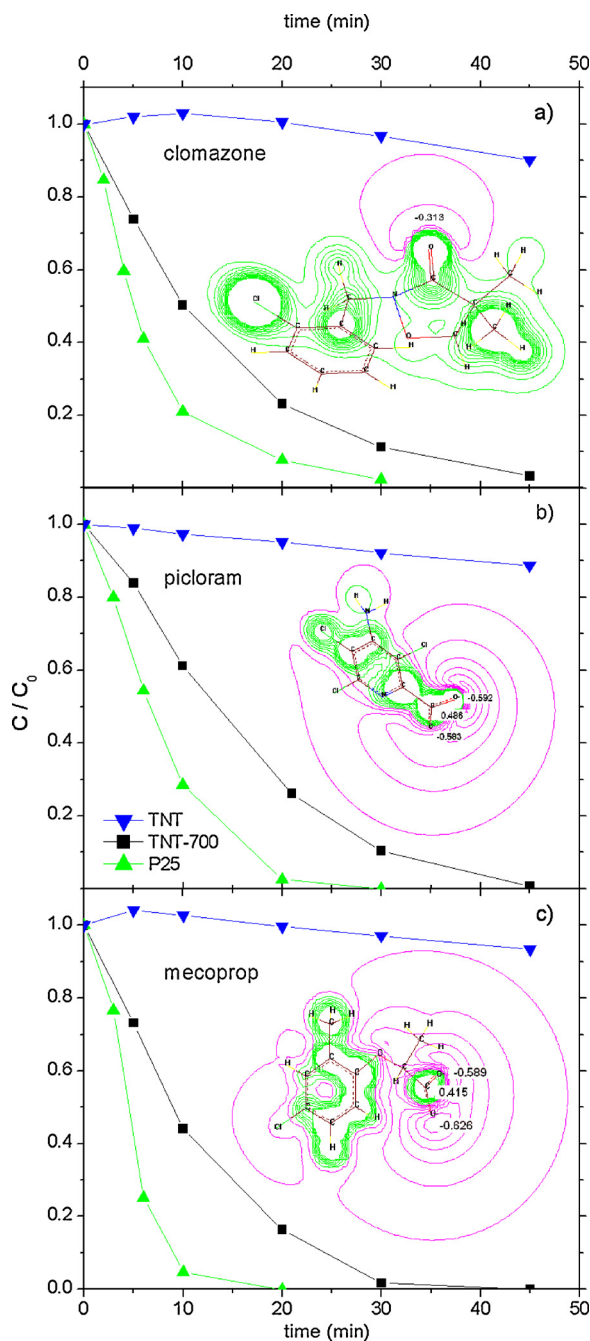


Fig. 7. Photocatalytic degradation of (a) clomazone, (b) picloram and (c) mecoprop using as prepared TNT, TNT-700 and P25 photocatalysts. MEP maps for the herbicide molecules are presented as insets. Electronegative and electropositive potential contours are shown in red and green lines, respectively. (For interpretation of the references to color in this figure legend, the reader is referred to the web version of the article.)

as prepared TNT samples had natural pH ~ 9 . On the other hand, in the evaluation of the photocatalytic degradation efficiency of chosen herbicides we also took into account their molecular structure. Hyperchem-derived MEP maps for the studied herbicide molecules with contribution of electronegative and electropositive potentials are shown in Fig. 7.

The as prepared titania nanotubes exhibited negligible photocatalytic activity, independently of molecular structure of studied herbicides, Fig. 7. Also, it was found that in the presence of as prepared titania nanotubes the adsorption of investigated herbicides were similar: about 2.6% for clomazone, $\sim 1.4\%$ for picloram and

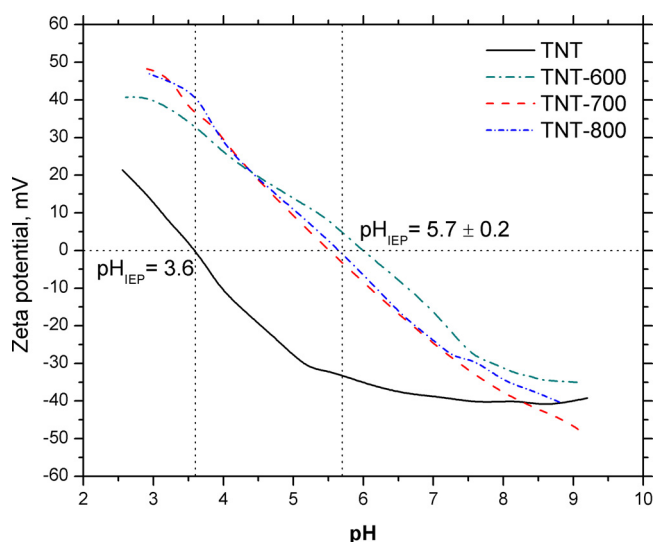


Fig. 8. Titration curves: ζ -potential vs pH for as prepared and annealed TNT materials.

$\sim 2.7\%$ for mecoprop. Mentioned results indicate that the larger surface area, which is a characteristic of nanotubes, does not necessarily yield higher photocatalytic activity, other factors, such as crystallinity domain, being of comparable if not of higher importance. Also, in the TNT sample at natural pH ~ 9 a significant number of surface sites are deprotonated, since the isoelectric point (pH_{IEP}) of titania nanotubes is 3.6, as can be seen in Fig. 8, which is in a good agreement with results of Bavykin et al. [31], yielding a negatively charged surface at working pH. TNT synthesized using alkaline hydrothermal procedure are negatively charged and interact with cationic species (amongst other species). Considering the negative electrostatic potential on the CO group in the molecule of clomazone, and COO^- groups of picloram and mecoprop, Fig. 6, the repulsion between the negatively charged surface of the catalyst and molecule substrate induced lower adsorption and consequently lower photocatalytic efficiency of titania nanotubes.

In the presence of titania nanotubes calcined at 700°C , the degradation efficiency of investigated herbicides generally increased in comparison to as prepared titania nanotubes, Fig. 6. TNT-700 had also negatively charged surface ($\text{pH}_{\text{IEP}} = 5.5$) (Fig. 8), as well as P25 ($\text{pH}_{\text{IEP}} = 6.2$) [21,32]. Considering degradation rates of selected herbicides, presented in Table 3, it could be concluded that there were no significant differences in photocatalytic activity of calcined sample. But, the overall increase in their photocatalytic activity in comparison to as prepared nanotubes is mainly the consequence of their generally higher crystallinity and existence of anatase and rutile phases (95%: 5%), which is a favorable condition (prerequisite) for the efficient photocatalytic degradation process on the surface of TiO_2 nanoparticles [29]. Taking into account negative electrostatic potential of studied molecules and the pH value of TNT 700 dispersions (7.2–7.8), it is clear that deprotonated surface of nanocrystals does not contribute significantly to increased efficiency of degradation process.

Table 3

The degradation rates (R) of selected herbicides determined at 10 min in the presence of P25 and TNT-700.

Catalyst	R ($\mu\text{mol}/(\text{dm}^3 \text{ min})$)		
	Clomazone	Picloram	Mecoprop
P25	7.05	6.35	15.8
TNT-700	3.4	2.5	4.1

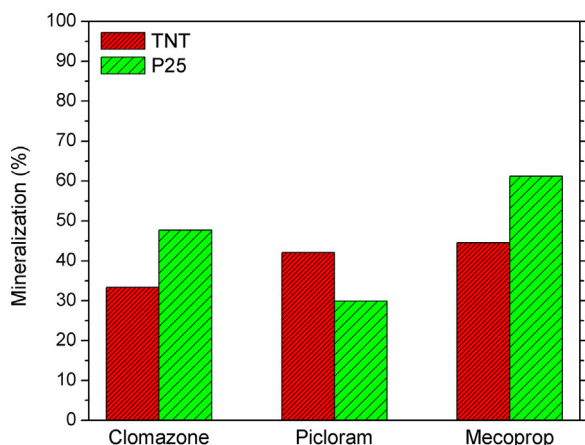


Fig. 9. The mineralization efficiency selected herbicides at 50 min of irradiation in presence P25 and TNT-700.

The photocatalytic activity of P25 was higher compared to the photocatalytic activity of titania nanotubes calcined at 700 °C in the degradation processes of chosen herbicides. Such result could be expected taking into account the presence of higher amount, approximately 25%, of rutile crystal phase in P25 in comparison to TNT 700. Also, the shape and dimension of P25 particles and consequently available surface area are favorable for more efficient photocatalytic degradation process.

Particularly high photocatalytic activity of P25 was observed for degradation of mecoprop. Degradation rate of mecoprop in the presence of P25 was about 4 times higher in comparison to degradation rate in the presence of TNT 700 sample. Also, the adsorption of mecoprop in presence P25 was slightly larger (6.2%) compared to clomazone (5.0%) and picloram (4.5%).

The presence of the electronegative COO[−] group, clearly shown in the Hyperchem-derived MEPs (Fig. 7) indicates that the negative electrostatic potential on the COO[−] group of mecoprop (Fig. 7c) is similar of picloram (Fig. 7b). At pH ~8.0 electrical forces are generated, i.e., the repulsion between the negatively charged surface of the catalyst and COO[−]. However, higher efficiency in the case of mecoprop degradation is probably due to the electron-donor or electron-withdrawing character of the different substituents in the herbicide aromatic/pyridine ring, which can activate/deactivate the ring with respect to the electrophilic attack of the •OH radical [33]. This may be explained in terms of the effect of CH₃ group as substituent. Namely, the higher reactivity of mecoprop compared to picloram is probably due to the presence of the benzene-ring activating CH₃ group (Fig. 7). On the other hand, since the herbicide mecoprop contain lateral chains and due to that is more hydrophobic than picloram which excludes stronger interaction with the TiO₂ surface, the higher degradation efficiency of mecoprop is probably the consequence of the efficient charge-transfer reactions at the expense of degradation by OH radical [34].

In order to obtain information about the degree of mineralization of selected herbicides in the presence of TNT-700 and P25 catalysts TOC measurements were done. The results showed that the efficiency of mineralization after 50 min of irradiation in the presence of TNT-700 samples were about 33, 42, and 44% for clomazone, picloram and mecoprop, respectively (Fig. 9). On the other hand, degree of mineralization in the presence of P25 was higher compared with TNT-700 except in the case of picloram (Fig. 9). It was found that for the same irradiation time was mineralized only 30% of picloram in presence P25.

Also, as can be seen in Fig. 9 the ratio of mineralization efficiency of clomazone in the presence of P25 and TNT-700 was similar as in the case of mecoprop (by the factor 1.4). However, as already

stated, difference in the rates of removal of the parent compound in the presence of the mentioned catalysts were higher (Table 3), i.e., in the case of clomazone and mecoprop ratio of removal rates were about 2 and 4, respectively. Based on these results, it can be concluded that the degradation of intermediates were more efficient in the presence of TNT-700. This effect is particularly pronounced in the case of picloram. Namely, the ratio of removal rate of picloram in presence P25 and TNT-700 was about 2.6, while the ratio of mineralization efficiency was only 0.7, i.e., the mineralization efficiency of picloram was higher in the presence of TNT-700. In some cases, during degradation of parent compound (herbicide) even more toxic intermediates are made in the degradation sequence. So, it is important to have such catalyst which can degrade efficiently pollutants down to their mineralization. Sometimes it is more important to have catalyst which can be more efficient when mineralization is in question then just efficient in removing parent pollutant. Although P25 is photocatalyst whose activity can rarely be reached by small-scale laboratory synthesized TiO₂, TOC results are more important than just rate of parent compound removal.

4. Conclusions

Titania nanotubes were successfully used for preparation of different elongated titania nanocrystals by annealing. Obtained samples had different shapes and sizes. With increasing temperature of calcination, aspect ratio of nanoparticles and their specific surface area decrease, degree of crystallinity increases as well as their photocatalytic activity. Photocatalytic activity of elongated nanocrystals reached max for TNT annealed at 700 °C. TNT annealed at 800 °C had slightly lower activity than TNT-700, but still much better than precursor material. This finding can be assigned to development of rutile crystalline phase during annealing, excluding the decisive influence of the particles shape. For our titania based materials the best ratio between anatase and rutile phase was 95:5%. Also the influence of molecular structure of the substrate was studied, following and comparing photocatalytic degradation of herbicides clomazone, picloram and mecoprop, using TNT-700 as photocatalyst. No significant influence of molecular structure was detected when the degradation rates of parent herbicides or their degree of mineralization (TOC) were compared. For herbicide picloram mineralization, TNT-700 was more effective than P25.

Acknowledgements

The authors are grateful to Dr Miodrag Mitrić for XRD, Prof. S.P. Ahrenkiel from South Dakota School of Mines & Technology, USA for TEM and Dr Bojan Jokić for FESEM measurements. We thank COST Action CM 1101 for support. Financial support for this study was granted by The Ministry of Education, Science and Technological Development of The Republic of Serbia, Projects: ON172056, ON172042 and III45020.

References

- [1] X. Chen, S.S. Mao, Chem. Rev. 107 (2007) 2891–2899.
- [2] M.A. Henderson, Surf. Sci. Rep. 66 (2011) 185–297.
- [3] Z. Ding, G.Q. Lu, P.F. Greenfield, J. Phys. Chem. B 104 (2000) 4815–4820.
- [4] J. Seo, H. Chung, M. Kim, J. Lee, I. Choi, J. Cheon, Small 3 (2007) 850–853.
- [5] H.J. Yun, H. Lee, J.B. Joo, W. Kim, J. Yi, J. Phys. Chem. C 113 (2009) 3050–3055.
- [6] J. Nian, H. Teng, J. Phys. Chem. B 110 (2006) 4193–4198.
- [7] T. Kasuga, M. Hiramatsu, A. Hoson, T. Sekino, K. Niihara, Langmuir 14 (1998) 3160–3163.
- [8] T. Kasuga, M. Hiramatsu, A. Hoson, T. Sekino, K. Niihara, Adv. Mater. 11 (1999) 1307–1312.
- [9] K. Kiatkittipong, A. Iwase, J. Scott, R. Amal, Chem. Eng. Sci. 93 (2013) 341–349.
- [10] N. Liu, X. Chen, J. Zhang, J.W. Schwank, Catal. Today 225 (2014) 34–51.
- [11] I.K. Konstantinou, D.G. Hela, T.A. Albanis, Environ. Pollut. 141 (2006) 555–570.
- [12] R. Venkatadri, R.W. Peters, Hazard. Waste Hazard. Mater. 10 (1993) 107–149.

- [13] S. Chiron, A. Fernandez-Alba, A. Rodriguez, E. Garcia-Calvo, E. Water Res. 34 (2000) 366–377.
- [14] B.F. Abramović, D.V. Šojić, in: I.A. Urboniene (Ed.), A Review. Desalination: Methods, Cost and Technology, Nova Science Publishers, Inc., New York, 2010, pp. 117–142.
- [15] S. Ahmed, M.G. Rasul, R. Brown, M.A. Hashib, J. Environ. Manage. 92 (2011) 311–330.
- [16] B.F. Abramović, V.N. Despotović, D.V. Šojić, D.Z. Orčić, J.J. Csanádi, D.D. Četojević-Simić, Chemosphere 93 (2013) 166–171.
- [17] D.B. Donald, A.J. Cessna, E. Sverko, N.E. Glozier, Environ. Health Perspect. 115 (2007) 1183–1191.
- [18] D.W. Hawker, J.L. Cumming, P.A. Neale, M.E. Bartkow, B.I. Escher, Water Res. 45 (2011) 768–780.
- [19] Z.V. Šaponjić, N.M. Dimitrijević, D.M. Tiede, A.J. Goshe, X. Zuo, L.X. Chen, A.S. Barnard, P. Zapol, L. Curtiss, T. Rajh, Adv. Mater. 17 (2005) 965–971.
- [20] A.V. Delgado, F. González-Caballero, R.J. Hunter, L.K. Koopal, J. Lyklema, J. Colloid Interface Sci. 309 (2007) 193–540.
- [21] K. Suttiponpanit, J. Jiang, M. Sahu, S. Suvachittanont, T. Charinpanitkul, P. Biswas, Nanoscale Res. Lett. 6 (2011) 27–33.
- [22] M.B. Yahia, F. Lemoigno, T. Beuvier, J.-S. Filhol, M. Richard-Plouet, L. Brohan, M.-L. Doublet, J. Chem. Phys. 130 (2009) 204501.
- [23] B. Poudel, W.Z. Wang, C. Dames, J.Y. Huang, S. Kunwar, D.Z. Wang, D. Banerjee, G. Chen, Z.F. Ren, Nanotechnology 16 (2005) 1935–1940.
- [24] L. Kőrösi, Sz. Papp, V. Hornok, A. Oszko, P. Petrik, D. Patko, R. Horvath, I. Dékány, J. Solid State Chem. 192 (2012) 342–350.
- [25] L. Kőrösi, Sz. Papp, E. Csapó, V. Meynen, P. Cool, I. Dékány, Micropor. Mesopor. Mater. 147 (2012) 53–58.
- [26] J. Yu, H. Yu, B. Cheng, C. Trapalis, J. Mol. Catal. A 249 (2006) 135–142.
- [27] M.B. Radoičić, I.A. Janković, V.N. Despotović, D.V. Šojić, T.D. Savić, Z.V. Šaponjić, B.F. Abramović, M.I. Čomor, Appl. Catal. B: Environ. 138–139 (2013) 122–127.
- [28] D. Cropek, P.A. Kemme, O.V. Makarova, L.X. Chen, T. Rajh, J. Phys. Chem. C 112 (2008) 8311–8318.
- [29] V. Pfeifer, P. Erhart, S. Li, K. Rachut, J. Morasch, J. Brötz, P. Reckers, T. Mayer, S. Rühle, A. Zaban, I.M. Seró, J. Bisquert, W. Jaegermann, A. Klein, J. Phys. Chem. Lett. 4 (2013) 4182–4190.
- [30] B.F. Abramović, S. Kler, D. Šojić, M. Laušević, T. Radović, D. Vione, J. Hazard. Mater. 198 (2011) 123–132.
- [31] D.V. Bavykin, E.V. Milsom, F. Marken, D.H. Kim, D.H. Marsh, D.J. Riley, F.C. Walsh, K.H. El-Abiary, A.A. Lapkin, Electrochem. Commun. 7 (2005) 1050–1058.
- [32] M. Qamar, M. Muneer, D. Bahnemann, J. Environ. Manage. 80 (2006) 99–106.
- [33] D.V. Šojić, V.N. Despotović, N.D. Abazović, M.I. Čomor, B.F. Abramović, J. Hazard. Mater. 179 (2010) 49–56.
- [34] J.F. Montoya, J.A. Velasquez, P. Salvador, Appl. Catal. B: Environ. 88 (2009) 50–58.